

Nanoscale crystal fabric of primary Ediacaran dolomite

Julia Wilcots¹, Pupa U. P. A. Gilbert², Kristin D. Bergmann¹

¹ Department of Earth, Atmospheric and Planetary Sciences, Massachusetts
Institute of Technology, Cambridge, MA

² Departments of Physics, Chemistry, Materials Science, Geoscience, University of
Wisconsin, Madison, WI

August 13, 2021

Abstract

The mineral dolomite ($\text{CaMg}(\text{CO}_3)_2$) forms in minor quantities in few modern sedimentary environments yet comprises the bulk of the Precambrian carbonate rock record. Precambrian dolomites are often preserved as fine-grained mudstone or in fabric-retentive forms, which possibly precipitated from minimally-altered seawater as primary cements or formed as replacements of primary CaCO_3 in early diagenetic environments. Direct evidence for primary dolomite precipitation from seawater in depositional environments has not yet been described. Here, we use synchrotron radiation to produce a nanoscale-resolution crystal orientation map of one ooid grain deposited at the onset of the Shuram carbon isotope excursion at ca. 574 Ma. In thin section, this ooid appears to preserve exquisite detail. Crystal orientation maps reveal small ($\sim 10 \mu\text{m}$) acicular, radially-oriented crystals grouped into bundles of similarly-oriented crystals that are variably length-fast and length-slow. We interpret that this petrographic fabric formed as the result of primary, spherulitic dolomite precipitation during ooid growth in shallow marine waters at ca. 574 Ma. This result provides additional evidence that the physicochemical properties of late Precambrian oceans promoted dolomite precipitation and supports a primary origin for the Shuram excursion.

1 Introduction

Carbonate rocks serve as the primary sink for carbon in the Earth system and preserve a record of the physical, chemical, and biological properties of marine settings throughout geologic time. The geological interpretation of carbonates through Earth history elucidate past changes in climate and carbon cycling, and also provide insight into potential future changes to the Earth system.

In Precambrian (>541 Ma) strata, carbonates are predominantly comprised of dolomite [4], and petrographic observations of these ancient dolomites commonly reveal fine, detail-preserving, and mimetic (fabric-retentive) crystal fabric [5, 12, 13, 22, 23]. Peculiarly, although modern seawater is supersaturated with respect to dolomite, aragonite (CaCO_3), not dolomite, is the carbonate mineral precipitated abiotically on modern marine shelves; dolomite can only be found forming on Earth’s surface today in unique hypersaline, hydrothermal, lacustrine, or biologically-mediated environments. The origin of Precambrian fabric-retentive dolomites and dearth of modern analogues has puzzled researchers for many decades — solving this “dolomite problem” would greatly advance our understanding of Earth during Precambrian time.

The finely crystalline petrographic fabrics common in Precambrian dolomites have been used as evidence to suggest that much of the Precambrian dolomite preserved in shallow-water carbonate successions formed in early diagenetic settings from seawater-like fluids [12, 15]. Early diagenetic, fabric-retentive dolomite is difficult to define mechanistically because many of the processes governing dolomite formation in shallow subsurface or surface-like settings are poorly constrained. Understanding how early diagenetic dolomite formed and whether it can be used as a faithful geochemical recorder of ancient seawater chemistry is crucial in the quest to reconstruct Precambrian environments.

The pursuit to explain fabric-retentive early diagenetic dolomite and thus better understand the Precambrian world has inspired the exploration of many mimetic dolomites of late Precambrian and early Paleozoic age. Petrographic evidence has been used to show that primary dolomite cements precipitated in pore space and cracks in Neoproterozoic-aged (1000-541 Ma) reefs [12, 13, 23], to interpret [5] and model [29] the mimetic replacement of aragonite by dolomite, and to suggest that Neoproterozoic fabric-retentive dolomites may have precipitated directly from seawater, instead of replacing original calcite or aragonite [22]. Early-forming dolomite appears more common in the late Precambrian, suggesting these Neoproterozoic seas had exceptional early (or primary) dolomite-forming potential.

Many prior petrographic studies have relied on ooids – spherical carbonate grains that form via precipitation from solution in high-energy shallow marine environments – as reliable petrographic indicators of primary mineralogy [5, 13, 19, 22]. Ooid mineralogies are nearly always interpreted as primary aragonite or calcite, not as primary dolomite. However, in some cases (most frequently in the Precambrian and particularly in the Neoproterozoic succession of Death Valley, USA), ooid fabrics are so pristinely preserved in dolomite that researchers have pondered whether they could represent primary dolomite precipitation [5, 22].

Here, we study one such exquisitely preserved dolomitc ooid sampled from the ca. 574 Ma Khufai Formation (Sultanate of Oman). This grain was deposited in a widespread 1-30 m thick oolite at the onset of the Shuram excursion, the largest negative carbon isotope excursion in the rock record, found in Ediacaran-aged shallow marine successions (635-541 Ma) worldwide [10]. Numerous hypotheses have been put forward to explain the genesis of the Shuram excursion; arguments for both a secondary and primary origin have been

proposed. A primary origin would likely require ~synchronous enigmatic environmental conditions across shallow water carbonate platforms [3, e.g.]; a secondary origin would require a significant diagenetic event at Shuram time [6, e.g.]. Intriguingly, the dolomitic oolite bed of the Khufai Formation, studied here, shares petrographic and sedimentologic similarities with a widespread dolomitic oolite found at the base of the Shuram excursion in the Johnnie Formation (Death Valley, USA) [3, 5], see Figures 1 and 2. Due to their commonly well-preserved crystal fabric, Johnnie Formation ooids have been interpreted as early diagenetic dolomitic replacement of primary aragonite [5], although they occur stratigraphically above similar ooids (of the Tonian Beck Spring Formation), that Tucker interpreted as primary dolomite.

Using synchrotron-based nanoscale crystal orientation mapping, electron backscatter diffraction (EBSD), and x-ray diffraction (XRD), we reveal the crystal morphology (size, shape, arrangement) and mineralogy of one ca. 574 Ma dolomitic ooid. We then interpret these observations in the context of previously proposed models of dolomite formation, prior petrographic studies of ooids, and the specific set of environmental conditions under which modern dolomite forms. We assess whether this ooid precipitated as an early diagenetic replacement of primary CaCO_3 or directly from seawater and discuss implications for the genesis of the Shuram excursion and properties of Precambrian shallow marine environments.

2 Formation models for fabric preserving dolomite

To establish a frame of reference in which to evaluate the fabric of our 574 Ma ooid, we characterize three models for the formation of fabric-retentive or primary dolomite from literature, each differentiable on the basis of crystal morphology, optical characteristics, and mineralogy. **Mimetic replacement dolomite:** In laboratory conditions, modern aragonite ooids are replaced with euhedral, microcubic (2-8 μm) dolomite crystals over 180 hours at 200°C [29]. Rhombohedral dolomite crystals faithfully preserve tangential ooid macrostructure, but do not preserve primary optical characteristics (pseudo-uniaxial cross) [29]. Notably, replacement begins on the outer surface of the ooid and progresses inward via micro pore spaces. **Precipitated primary dolomite:** Primary dolomite cements line pore spaces in Neoproterozoic carbonates [13]. Individual crystals have a variety of forms, but are generally fibrous or bladed in shape, form bundles that fan out from their nucleation site, have an invariably length-slow optical characteristic, and can grow up to ca. 2mm long [12, 13]. **Precipitated primary protodolomite:** In laboratory conditions at high temperatures (60-200°C) and high dolomite supersaturation, protodolomite precipitates as nanocrystalline spherulites [18]. The poorly ordered protodolomite precursor transforms to ordered dolomite comprised of larger (>100 nm), planar crystals over hours to days. Protodolomite forming in modern surface environments in close association with microbial communities can also be spherulitic [25].

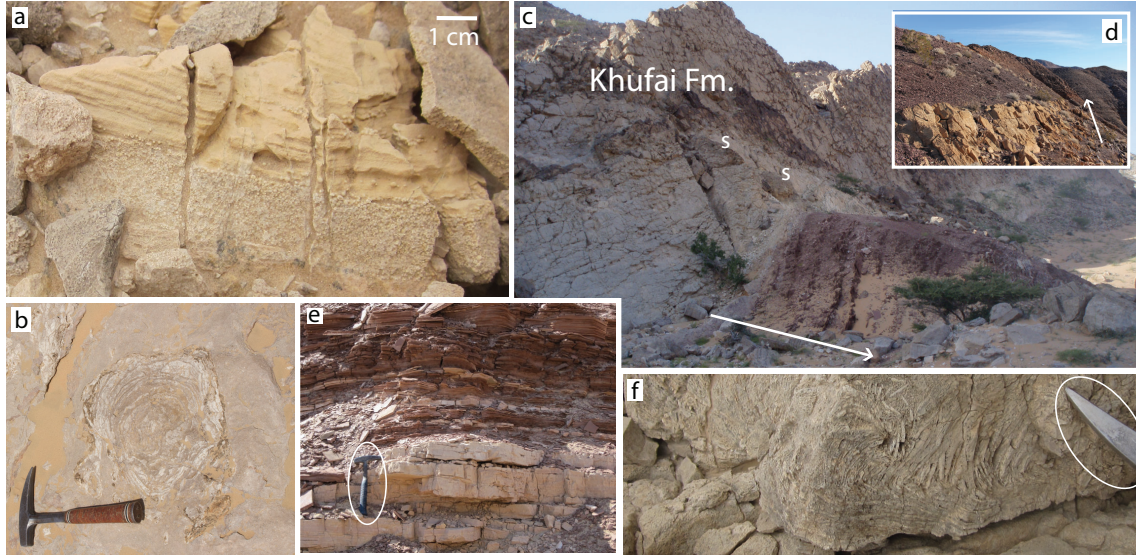


Figure 1: Field photos of the Khufai (Oman) and Johnnie (USA) Formations. **a:** Khufai oolite overlain by cross-stratified, upward fining dolostone. **b:** Cross-section of a stromatolite within the Khufai oolite (plan view). Hammer for scale. **c:** Khufai Formation and overlying red silts of the Shuram Formation, as exposed in Mukhaibah Dome (see [2, 16]). Arrow points to stratigraphic up, ‘s’ denote stromatolitic bioherms within Khufai oolite. **d:** The Khufai-equivalent Johnnie oolite (Death Valley, USA) is also overlain by red silts. Arrow points to stratigraphic up. **e:** Detailed view of the Khufai-to-Shuram gradational transition, Mukhaibah Dome, Oman. Hammer for scale. **f:** Rip-up clasts in stromatolitic facies within Khufai oolite. Hammer pick for scale.

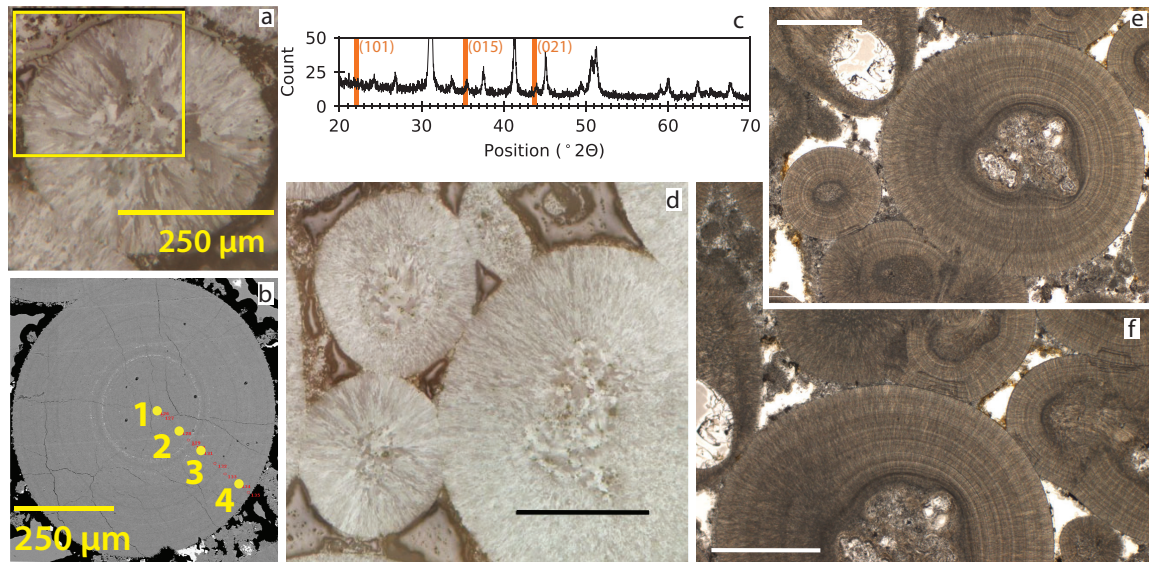


Figure 2: Petrographic images and mineralogy of the Khufai Formation oolite. **a:** Reflected light image. Yellow boxed region was PIC-mapped at 20 μ m resolution (shown in Figure 3a). **b:** Locations of electron probe micro analysis in a representative ooid within the Khufai oolite. CaO/MgO ratios in spots 1-4 are 21.8/13.2, 21.9/13.1, 22.3/12.7, and 21.8/13.0, respectively. **c:** XRD spectrum of the same oolite. Orange lines indicate dolomite ordering peaks [14]. **d:** Reflected light image from the same hand sample as **a**. **e, f:** Thin section images of other ooids from the same bed in the uppermost Khufai Fm. Ooids in **d, e, f** all show the same novel dolomite crystal structure we observe and describe in detail for the ooid in **a** and Figure 3. Scale bars are 500 μ m unless otherwise noted.

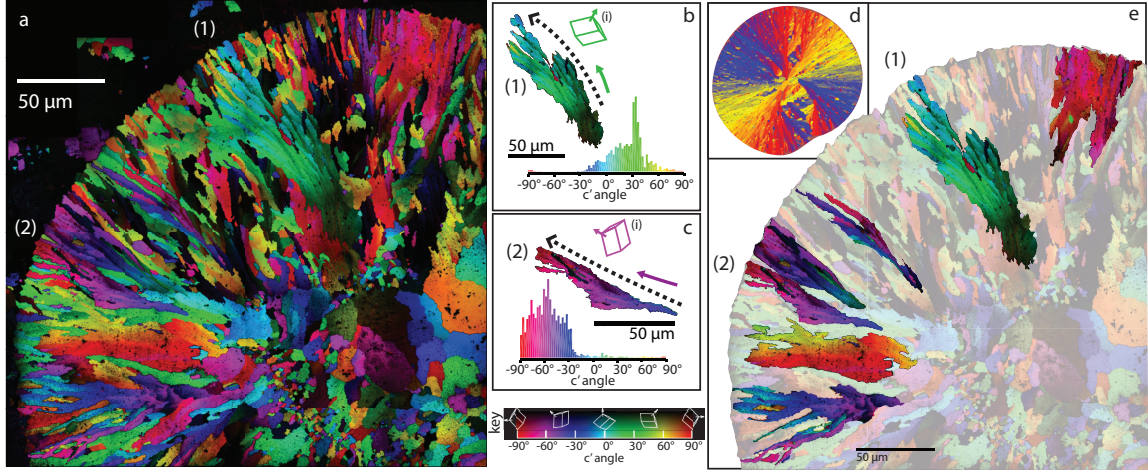


Figure 3: Crystal orientation maps of a fabric-retentive, Ediacaran, dolomitic ooid. **a**: Polarization-dependent Imaging Contrast (PIC) map of the upper quadrant of the ooid shown in Fig. 2a. Each colored region corresponds to one crystal. Colors and brightness represent in-plane (c' -axis) and out-of-plane orientations, respectively, as depicted by the dolomite rhombs and color bar in (labelled “key”). **b**, **c**: Two bundles of similarly-oriented crystals extracted from the PIC map in **a**, **e** (labeled (1), (2)). Histograms of pixel colors within each bundle show that all crystals within each bundle are similarly oriented. In each case, bundle elongation (dashed lines) and crystal length (solid arrows) are cooriented. Mode crystal orientation for each bundle is depicted by the sketched dolomite rhombs ((i), colored accordingly). The purple bundle, (2), is length-fast; the green bundle, (1), is length-slow. **d**: A modeled spherulitic form [11] resembles the PIC map in **a**, including plumose bundles, abrupt misorientations, and bundles that terminate at the edge of the form. **e**: Highlighted view of some of the plumose, quasi-spherulitic bundles of similarly-oriented crystals observed in **a**.

3 Novel crystal structure of a ca. 574 Ma dolomite ooid

Recognizing the value of petrographic observations in the classification of ancient dolomites, we leverage the nanoscale resolution of synchrotron-based Polarization-dependent Imaging Contrast (PIC) mapping to produce a high-resolution map of crystal orientations and geometries within a ca. 574 Ma dolomitic ooid that appears exquisitely fabric-retentive in thin section (Fig. 2). Using soft x-rays with variable linear polarization angle, PIC mapping measures the c-axis orientations of nanocrystals and displays them in 3D, at 20nm resolution, using color: hue and brightness represent in- and out-of-plane angles, respectively (see Methods) [8]. Since PIC mapping is based on x-ray linear dichroism — a physical effect that depends on bond angle orientation and crystal structure — its prior observation and use in aragonite, calcite, and vaterite minerals [7] predicts that it also works for dolomite, as demonstrated here for the first time.

PIC mapping reveals that this ooid, like most ooids, is comprised of an outer cortex which formed around an inner nucleus (Fig. 3) [1]. Here, the cortex is dominantly comprised of small acicular (needle-shaped) crystals, while crystals in the nucleus are generally larger and equant. We highlight six observations of the outer cortex that together describe a novel dolomite crystal fabric: (1) Individual dolomite crystals are small ($\sim 2\mu\text{m}$ by $15\mu\text{m}$), acicular, radial, and non-planar [20]. (2) Some crystals are grouped into bundles of similarly-oriented crystals (Fig. 3b, c, e). (3) While crystals within each bundle maintain similar orientations (Fig. 3), the optical characteristics of crystals differ between bundles: some are length-fast, with the c-axes pointing along the same vector as the bundle (purple, Fig. 3c) while others are length-slow, with the c-axes pointing perpendicular to the bundle orientation (green, Fig. 3b). (4) Bundles have a curved, plumose morphology that become more expansive towards the edge of the ooid. (5) Most plumose spherulitic bundles terminate at the curved outer edge of the ooid. (6) Textbook Mg:Ca ratios from EPMA (Fig. 2b) and the presence of the (015) and (021) ordering peaks [14] in the XRD spectrum (Fig. 2c) indicate that this ooid is comprised of stoichiometric, ordered dolomite: Ca and Mg are present in equal parts within the carbonate lattice within coherent cation-specific planes.

This combination of features is not completely described by any one of the literature-derived models for fabric-retentive dolomite detailed above, but has some similarities to each. The mimetic replacement model is supported by the EMPA and XRD results and the observed small crystal size, but our ooid's crystals are not rhombohedral. The primary dolomite cement model is supported by this ooid's acicular crystals that form fan-like bundles, but unlike published length-slow examples [12, 13], ooid crystal bundles are variably length-slow and length-fast. The primary protodolomite model is supported by the space filling, radial, elongate crystals arranged in plumose bundles, which show many similarities to documented protodolomite [18], microbially-mediated [25], and modeled [11] (see Fig 3d) spherulites. Yet, true spherulites always have straight crystals with length-fast orientations, like in plumose spherulite bundles observed in coral skeletons using PIC mapping [21]. Thus the curved crystals and bundles, variable length-slow and length-fast crystal

orientations and the stoichiometric, ordered composition are together inconsistent with the protodolomite model [18]. The spherulite-like crystal bundle morphology we observe – including the consistent optical characteristics of individual bundles and their plumose geometry – along with the preponderance of bundle terminations at the ooid edge, imply the plumose bundles (e.g. Fig. 3e) grew synchronously during ooid formation.

Our observations show this ooid has the most in common with spherulitic protodolomite and Neoproterozoic dolomite cements: both primary precipitates. However, the variably length-slow and -fast, curved, plumose bundles described here present a novel dolomite crystal morphology. We thus suggest this ooid represents a new crystal fabric formed by primary precipitation of dolomite from seawater.

3.1 Implications for Precambrian environments

With the above evidence that this ooid grew as primary dolomite, it is important to consider its broader depositional context in the ca. 574 Ma Khufai Formation and to use this geologic context to infer the environmental conditions in which this ooid formed. Field sedimentological observations show our ooid is sampled from a cross-stratified ooid-intraclast grainstone deposited in a high-energy, shallow marine setting [16], 1. As stated above, this oolite was deposited at the onset of the Shuram excursion; $\delta^{13}C_{VPDB}$, $\delta^{18}O_{VPDB}$, and the carbonate clumped isotope temperature ($T_{\Delta 47}$) of the same sample we PIC mapped are -2.8‰ , -7.8‰ , and $66 \pm 23^\circ\text{C}$ (2 S.E.), respectively (see Table 3, sample MD6 258.6 in [2]). Sulfur isotope values measured at the same interval are highly variable, falling “dramatically” from a peak of $\delta^{34}S_{CAS} = 35\text{‰}$ at the onset of the Shuram excursion [17]. To further evaluate our petrographic observation-based hypothesis that this ooid represents primary dolomite precipitation and to further constrain the properties of this ca. 574 Ma shallow marine environment, we can turn to the few modern dolomite analogues that exist and ask whether the Khufai Formation could represent a similar depositional environment.

In the modern, dolomite does form in shallow water environments under specific, localized conditions often in lagoons, sabkha, or lake settings. For example, in the Coorong lakes of South Australia, fine grained ($<1\text{ }\mu\text{m}$ - $20\text{ }\mu\text{m}$), spherulitic dolomite precipitates during the hottest, most evaporitic portion of the year in high-salinity, high pH, high $[\text{Mg}^{2+}]$ settings dominated by sulfate-reducing bacteria [28]. Calculated dolomite precipitation temperatures (from $\delta^{18}O$) fall between ~ 40 and $\sim 90^\circ\text{C}$, depending on sample location and $\delta^{18}O$ temperature calibration (see Figure 9 in [28]) and $\delta^{34}S_{V-CDT}$ measured on lakewater precipitates varies between 25 and 30‰. In Lagoa Vermelha, Brazil, Ca-rich dolomite with depleted $\delta^{13}C$ (-7.49 to -8.98 ‰) forms in anoxic, hypersaline conditions dominated by sulfate-reducing bacteria at the sediment-water interface [24, 26]. This primary precipitated dolomite then “ages” in the anoxic sediment column ($<1\text{m}$ depth) to a more stoichiometric, ordered form [24, 26].

While neither the Coorong Lakes nor Lagoa Vermelha dolomites can be taken as perfect analogues for the Khufai Formation (no ooids have been found in either location),

the geochemical and physical properties of these exemplary modern locales have much in common with the Khufai oolite, lending support to our hypothesis that the ooid studied here formed via primary precipitation from solution. The presence of sulfur-reducing bacteria is thought to be critical to dolomite formation in both modern examples, and has been identified in laboratory studies as a potential mechanism (through the production of dissolved sulfide and subsequent disruption of Mg^{2+} -water complexes) for the precipitation of dolomite in the geologic record (see, for example, [30]). We suggest that warm water temperatures, periodically evaporitic conditions, the presence of dissolved sulfide and sulfate-reducing bacteria, and a source of Mg^{2+} ions [9, 27], could have combined to create a shallow marine environment conducive to the precipitation of dolomite in the late Ediacaran period. Similarities in ooid petrography and stratigraphy between the Shuram-aged successions in Death Valley [3, 5, 22] and Oman ([2, 16] and this study) suggest that these favorable dolomite conditions may have been widespread across shallow marine platforms around 574 Ma.

Methods

Sample preparation

All of the analyses described here were conducted on parts of one hand sample (ca. 10 by 10 cm) of oolite collected by K. Bergmann from the upper Khufai Formation, Sultanate of Oman (MD6 258.6, see [2, 16]). To prepare for PIC mapping, the sample was cut down to a 4mm^3 cube, polished and coated with 1nm of Pt following [21]. A second cut of the sample was thin sectioned, finished with a microprobe-quality polish to $0.25\mu\text{m}$ and carbon coated for electron probe spot analysis (Fig. 2b). For X-ray diffraction (Fig. 2c), a third section of the oolite sample was powdered using a drill press [2].

Polarization-dependent Imaging Contrast (PIC) Mapping

We collected the data displayed in the PIC map in Fig. 3 on beamline 11.0.1.1 at the Advanced Light Source, Lawrence Berkeley National Laboratory, using X-ray PhotoEmission Electron spectroMicroscopy (X-PEEM). The polished sample was mounted such that incident X-ray beams hit the sample at a 60° incident angle. Working at a fixed photon energy of 534 eV (π^* peak in carbonate oxygen K-edge spectra), the linear polarization was rotated at the undulator source from 0° to 90° at 5° increments. Each of the resulting 19 images (one at each 5° increment) were stacked and analyzed using GG Macros (see [21]). In each pixel of the stack, the intensity (I) vs. polarization angle (χ) curve was fitted using a cosine-squared function: $I = a + b\cos^2(\chi - c')$ (Malus's law) with three fit parameters – a , b and c' – where c' is the in-plane and b/a the out-of-plane angle of the crystal c-axis orientation, displayed by hue and brightness as shown by the color legend in Fig. 3 [8, 7]. This process was repeated for a series of 56 by $56\mu\text{m}$ areas with 56nm pixels partly over-

lapping to cover the entire quadrant of the ooid outlined in Fig. 2a. The ~ 50 images were then stitched together using Adobe Photoshop CC 2017 to produce the PIC map shown in Fig. 3a. Together, the hue and brightness of each pixel in a PIC map completely describe the three-dimensional orientation of a crystal's c-axis at the same coordinates as the pixel.

X-ray diffraction (XRD)

Oolite powder was analyzed on the PANalytical X'Pert Pro in the Material Science Department at the California Institute of Technology by [2]. Scans were run from $5-70^\circ 2\theta$ with a step size of 0.008 and a scan step time of 10.16 s. A Cu anode was used at 45 kV and 40 mA. A zero-background silicon plate was used for all measurements. Mineralogical phases were initially identified using the X'Pert Highscore IDMin function in Jade.

Electron probe microanalysis (EPMA)

Electron probe spot analyses, shown in Fig. 2b, were taken using a JEOL JXA-8200 Electron Microprobe at the California Institute of Technology with an accelerating voltage of 15 kV, beam current of 20 nA, and beam size of 1 μm . Calcite and dolomite standards were used to calibrate the Ca and Mg measurements, respectively. Average detection limits for Ca and Mg were 177 ppm and 283 ppm, respectively. The CITZAF method was used for matrix correction.

Acknowledgements

JW thanks C. Sun for help with sample preparation at UW-Madison and PIC mapping at LBNL. KDB thanks M. Osburn, J. Grotzinger and W. Fischer for field and laboratory support. oolite, and C. Ma for EPMA assistance. PG acknowledges 80% support from the U.S. DOE, Office of Science, Office of Basic Energy Sciences, Chemical Sciences, Geosciences, and Biosciences Division, under Award DE-FG02-07ER15899, and 20% support from NSF grant DMR-1603192. PEEM experiments were done at the Advanced Light Source, supported by beamline scientist R. Chopdekar, and the Director, Office of Science, Office of Basic Energy Sciences, US DOE under Contract No. DE-AC02-05CH11231. Additional funding was provided by the Packard Foundation to KDB.

References

- [1] Anderson, N. T., Cowan, C. A., and Bergmann, K. D. (2020). A case for the growth of ancient ooids within the sediment pile. *Journal of Sedimentary Research*, 90(8):843–854.
- [2] Bergmann, K. D., Al Balushi, S. A. K., Mackey, T. J., Grotzinger, J. P., and Eiler,

- J. M. (2018). A 600-million-year carbonate clumped-isotope record from the Sultanate of Oman. *Journal of Sedimentary Research*, 88(August):960–979.
- [3] Bergmann, K. D., Zentmyer, R. A., and Fischer, W. W. (2011). The stratigraphic expression of a large negative carbon isotope excursion from the Ediacaran Johnnie Formation, Death Valley. *Precambrian Research*, 188(1-4):45–56.
- [4] Cantine, M. D., Knoll, A. H., and Bergmann, K. D. (2020). Carbonates before skeletons: A database approach. *Earth-Science Reviews*, 201:103065.
- [5] Corsetti, F. A., Kidder, D. L., and Marenco, P. J. (2006). Trends in oolite dolomitization across the Neoproterozoic-Cambrian boundary: A case study from Death Valley, California. *Sedimentary Geology*, 191(3-4):135–150.
- [6] Derry, L. A. (2010). A burial diagenesis origin for the Ediacaran Shuram–Wonoka carbon isotope anomaly. *Earth and Planetary Science Letters*, 294(1-2):152–162.
- [7] DeVol, R. T., Metzler, R. A., Kabalah-Amitai, L., Pokroy, B., Politi, Y., Gal, A., Addadi, L., Weiner, S., Fernandez-Martinez, A., Demichelis, R., et al. (2014). Oxygen spectroscopy and polarization-dependent imaging contrast (pic)-mapping of calcium carbonate minerals and biominerals. *The Journal of Physical Chemistry B*, 118(28):8449–8457.
- [8] Gilbert, P. U. P. A., Young, A., and Coppersmith, S. N. (2011). Measurement of c-axis angular orientation in calcite (CaCO_3) nanocrystals using X-ray absorption spectroscopy. *Proceedings of the National Academy of Sciences*, 108(28):11350–11355.
- [9] Given, R. K. and Wilkinson, B. H. (1987). Dolomite abundance and stratigraphic age; constraints on rates and mechanisms of Phanerozoic dolostone formation. *Journal of Sedimentary Research*, 57(6):1068–1078.
- [10] Grotzinger, J. P., Fike, D. A., and Fischer, W. W. (2011). Enigmatic origin of the largest-known carbon isotope excursion in Earth’s history. *Nature Geoscience*, 4(5):285–292.
- [11] Hendler, N., Mentovich, E., Korbuly, B., Pusztai, T., Gránásy, L., and Richter, S. (2015). Growth control of peptide-nanotube spherulitic films: Experiments and simulations. *Nano Research*, 8(11):3630–3638.
- [12] Hood, A. S., Wallace, M. W., and Drysdale, R. N. (2011). Neoproterozoic aragonite-dolomite seas? Widespread marine dolomite precipitation in Cryogenian reef complexes. *Geology*, 39(9):871–874.
- [13] Hood, A. v. S. and Wallace, M. W. (2018). Neoproterozoic marine carbonates and their paleoceanographic significance. *Global and Planetary Change*, 160(November 2017):28–45.

- [14] Kaczmarek, S. E., Gregg, J. M., Bish, D. L., Machel, H. G., Fouke, B. W., MacNeil, A., Lonnee, J., Wood, R., et al. (2017). Dolomite, very-high magnesium calcite, and microbes: implications for the microbial model of dolomitization. In *Characterization and Modeling of Carbonates–Mountjoy Symposium*, volume 1, pages 7–20.
- [15] Knoll, A. and Swett, K. (1990). Carbonate deposition during the late Proterozoic Era: an example from Spitsbergen. *American Journal of Science*, 290:104–132.
- [16] Osburn, M., Grotzinger, J., and Bergmann, K. (2014). Evolution of a middle Ediacaran carbonate ramp: Khufai Formation, Sultanate of Oman. *AAPG Bulletin*, 98(8):1631–1667.
- [17] Osburn, M. R., Owens, J., Bergmann, K. D., Lyons, T. W., and Grotzinger, J. P. (2015). Dynamic changes in sulfate sulfur isotopes preceding the Ediacaran Shuram Excursion. *Geochimica et Cosmochimica Acta*, 170:204–224.
- [18] Rodriguez-Blanco, J. D., Shaw, S., and Benning, L. G. (2015). A route for the direct crystallization of dolomite. *American Mineralogist*, 100(5-6):1172–1181.
- [19] Sandberg, P. A. (1975). New interpretations of Great Salt Lake ooids and of ancient non-skeletal carbonate mineralogy. *Sedimentology*, 22:497–537.
- [20] Sibley, D. F. and Gregg, J. M. (1987). Classification of dolomite rock textures. *Journal of Sedimentary Research*, 57(6):967–975.
- [21] Sun, C. Y., Marcus, M. A., Frazier, M. J., Giuffre, A. J., Mass, T., and Gilbert, P. U. (2017). Spherulitic Growth of Coral Skeletons and Synthetic Aragonite: Nature’s Three-Dimensional Printing. *ACS Nano*, 11(7):6612–6622.
- [22] Tucker, M. E. (1982). Precambrian dolomites: Petrographic and isotopic evidence that they differ from Phanerozoic dolomites. *Geology*, 10(January):7–12.
- [23] Tucker, M. E. (1983). Diagenesis, geochemistry, and origin of a Precambrian dolomite; the Beck Spring Dolomite of eastern California. *Journal of Sedimentary Research*, 53(4):1097–1119.
- [24] Vasconcelos, C. and McKenzie, J. A. (1997). Microbial mediation of modern dolomite precipitation and diagenesis under anoxic conditions (lagoa vermelha, rio de janeiro, brazil). *Journal of sedimentary Research*, 67(3):378–390.
- [25] Vasconcelos, C., McKenzie, J. A., Bernasconi, S., Grujic, D., and Tiens, A. J. (1995). Microbial mediation as a possible mechanism for natural dolomite formation at low temperatures. *Nature*, 377(6546):220–222.

- [26] Vasconcelos, C., Warthmann, R., McKenzie, J. A., Visscher, P. T., Bittermann, A. G., and van Lith, Y. (2006). Lithifying microbial mats in Lagoa Vermelha, Brazil: modern Precambrian relics? *Sedimentary Geology*, 185(3-4):175–183.
- [27] von der Borch, C. C., Lock, D. E., and Schwebel, D. (1975). Ground-water formation of dolomite in the Coorong region of South Australia. *Geology*, 3(5):283–285.
- [28] Wacey, D., Wright, D. T., and Boyce, A. J. (2007). A stable isotope study of microbial dolomite formation in the Coorong Region, South Australia. *Chemical Geology*, 244(1-2):155–174.
- [29] Zempolich, W. G. and Baker, P. A. (1993). Experimental and natural mimetic dolomitization of aragonite ooids. *Journal of Sedimentary Research*, 63(4):596–606.
- [30] Zhang, F., Xu, H., Konishi, H., Kemp, J. M., Roden, E. E., and Shen, Z. (2012). Dissolved sulfide-catalyzed precipitation of disordered dolomite: Implications for the formation mechanism of sedimentary dolomite. *Geochimica et Cosmochimica Acta*, 97:148–165.